Int. J. Electrochem. Sci., 15 **(2020)** 11316 – 11325, doi: 10.20964/2020.11.67

International Journal of
ELECTROCHEMICAL
SCIENCE
www.electrochemsci.org

Effect of Nd_2O_3 and CeO_2 co-doping on the Dielectric Properties of $Ba_{0.94}Ca_{0.06}Ti_{0.90}Sn_{0.10}O_3$ Lead-Free Ceramics

Zhi-wei Li[1], *Ming-gang Ma*[3], *Cheng-bo Li*[3], *Zhi-hui Chen*[2*], *Jiu-jun Xu*[1*]

[1] Department of Materials Science and Engineering, Dalian Maritime University, Dalian, Liaoning 116026, China;
[2] School of Materials Science and Engineering, Changzhou University, Changzhou, 213164, Jiangsu, China;
[3] Benxi Iron and steel Company Limited, Benxi, 117100, Liaoning, China
[*]E-mail: jjxu@dlmu.edu.cn;

Received: 21 July 2020 / *Accepted:* 8 September 2020 / *Published:* 30 September 2020

The $Ba_{0.94}Ca_{0.06}Ti_{0.90}Sn_{0.10}O_3$ lead-free piezoelectric ceramics co-doped with 0.03mol%CeO_2 and Nd_2O_3 (BCTS-Ce-xNd_2O_3, x=0, 0.01, 0.02, 0.03, 0.04, 0.05) were prepared by solid-state sintering method at 1410°C. The effects of Nd_2O_3 on phase structure, microstructure and electrical properties were investigated. The X-ray diffraction (XRD) analysis indicates that single perovskite structures were obtained. The tetragonal and rhombohedral phases coexisted in the composition with x=0.02-0.05. SEM images reveal that the grain sizes of the samples decreased from 68.7 μm to 17.1 μm with x increasing. The optimized piezoelectric properties were obtained at x=0.03 with piezoelectric coefficient of 578 pC/N and planar electromechanical coupling factor of 49.0%. Diffuse phase transition behavior of the samples was weakened by the addition of Nd_2O_3.

Keywords: $BaTiO_3$; Dielectric properties; Piezoelectric properties; Nd_2O_3 and CeO_2 co-doping

1. INTRODUCTION

The piezoelectric materials which convert mechanical energy into electrical energy are widely used in commercial capacitors due to their advantages over batteries such as low cost and effective volume to store energy [1-3]. As one member of lead-free piezoelectric materials [4-5], $BaTiO_3$ based ceramics with typical ABO_3 structure have been extensively studied for their superior dielectric constant, ferroelectric activity and nonlinear optical coefficients [6-8]. However, the low piezoelectric properties restrict their real applications. A high performance (Ba,Ca)(Ti,Sn)O_3 system with piezoelectric coefficient of d_{33} up to 578pC/N was developed by co-doping of Ca^{2+} and Sn^{4+} into the $BaTiO_3$ structure [9-13]. In the new system, phase transition from rhombohedral phase to tetragonal phase results in a

strong temperature dependence of piezoelectric properties. On the other hand, doping with rare earth ions such as Er^{3+} [14,15], Y^{3+} [16, 17], La^{3+} [18, 19] in piezoelectric ceramics including $BaTiO_3$, $Bi_{0.5}Na_{0.5}TiO_3$ and $(Bi_{0.5}Na_{0.5})_{0.94}Ba_{0.06}TiO_3$ system were reported to be effective to improve the electrical properties by downshifting phase transition temperature, decreasing grain sizes and tailoring microstructures. Generally, the optimization of piezoelectric properties is related to homogeneous microstructures. CeO_2 as a sintering aid of tetravalent oxide is commonly used to improve microstructures of lead-free ceramics, such as $BaTiO_3$ and $(Ba,Ca)(Ti,Sn)O_3$[20, 21]. In our previous work, $Ba_{0.94}Ca_{0.06}Ti_{0.90}Sn_{0.10}O_3$ (abbreviated as BCTS) ceramics were obtained at 1420°C by the addition of 0.03mol%CeO_2, where the sintering temperature was decreased without sacrificing the electrical properties of the ceramics (d_{33}=541pC/N). The optimized dielectric properties with high dielectric constants and low dielectric loss also exhibit wide application prospect of the CeO_2 doped $(Ba,Ca)(Ti,Sn)O_3$ ceramics in multilayer ceramic capacitor (MLCC) [22]. As another light rare earth oxide, Nd_2O_3 was also reported to modify the structure and dielectric properties of $BaTiO_3$-based ceramics [23-24]. As reported in literature, Nd_2O_3 addition can promote the formation of internal deformation/distortion of the TiO_6 octahedra and Nd^{3+}-barium vacancies, and also decrease the temperature of the dielectric maximum as well as the grain size [25]. However, as far as we know, few papers have been reported to discuss the co-doping of lead-free BCTS ceramics by CeO_2 and Nd_2O_3.

In this work, BCTS lead-free ceramics co-doped by CeO_2 and Nd_2O_3 were prepared and the multi-modification effects of (Ce, Nd) on the microstructure and the electrical properties were discussed.

2. EXPERIMENT

$Ba_{0.94}Ca_{0.06}Ti_{0.90}Sn_{0.10}O_3$-0.03mol%$CeO_2$-xmol%$Nd_2O_3$ ceramics (abbreviated as BCTS-Ce-xNd_2O_3, x=0, 0.01, 0.02, 0.03, 0.04, and 0.05) were prepared by conventional solid-state sintering method. The starting ingredients $BaCO_3$ (99.9%), $CaCO_3$ (99.9%), TiO_2 (99.9%), SnO_2 (99.5%), CeO_2 (99.5%) and Nd_2O_3 (99.8%) were weighed stoichiometrically, and the powers were mixed for 1h in the ethanol using an agate mortar. The mixture was calcined at 1200°C for 4h in air and subsequently milled again, then pressed into 11 mm-diameter pellets with the addition of 8 wt% polyvinyl alcohol (PVA). The pellets were heated at 550°C for 2h to burn out the PVA binder, then sintered at 1410°C for 2h.

X-ray diffractometer (XRD, Rigaku D/max-2500/PC, Japan) with Cu $K_{\alpha 1}$ radiation (λ=1.5406Å) was used to carry out the phase analysis of the sintered samples. Microstructures of the ceramics were observed by Scanning electron microscope (SEM, HITACHI S-4300) after thermally etched at 1200°C for 1h. The unit cell volumes of the samples were calculated from the diffraction data refined by the Wincell and Winplote software. The densities of the ceramics were measured using Archimedes' method. The sintered pellets were well polished on both sides, on which, silver paste was coated and fired at 650°C for 30 min as electrodes to perform electrical property measurements. Dielectric properties were measured at different frequencies in the temperature range from 30°C-110°C using a computer-controlled TH2818 Automatic Component Analyzer (Changzhou Tonghui Electronic Co., Ltd., China). The specimens were polarized under an electric field of 3.5 kV/mm with an interval of 0.5 kV/mm for 15 min in silicon oil at room temperature. The corresponding piezoelectric constant was measured by a

quasi-static d_{33} meter (ZJ-3AN, China), and the planar coupling coefficient K_p was obtained by Agilent 4294A impedance analyze. Polarization-electric field (P–E) hysteresis loops of the samples were measured by a Radiant Precision Premier LC ferroelectric material test system (Radiant Technologies Inc., USA).

3. RESULTS AND DISCUSSION

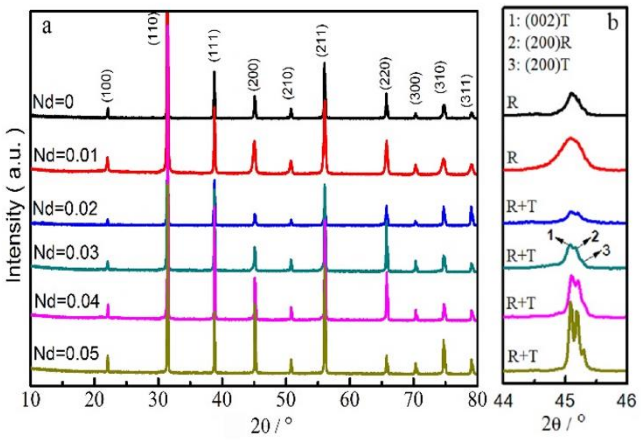

Figure 1. The XRD patterns of the BCTS-Ce-xNd_2O_3 ceramics with x=0 to 0.05. (a) 2θ=10°-80°; (b) Enlarged pattern from 44° to 46°

Fig. 1 shows the XRD patterns of the BCTS-Ce-xNd_2O_3 ceramics (x=0-0.05). All the samples exhibit single perovskite-type structures from 10° to 80° (**Fig. 1a)**, indicating that Nd^{3+} ions diffused into the crystal lattice. The diffraction peaks of the samples with x=0 to 0.01 demonstrate a pure rhombohedral phase characterized with a single symmetric peak for the (200) plane at a 2θ angle of approximately 45° (**Fig. 1b)**. The single peak (200) became asymmetric and appeared spitting trend with increasing x. The mixed peaks consisted of three curves from left to right signify the peaks for (002)T, (200)R and (200)T, respectively, indicating the coexistence of rhombohedral and tetragonal phases (PDF#79-2264) at the composition range from x=0.02 to 0.05 [23].

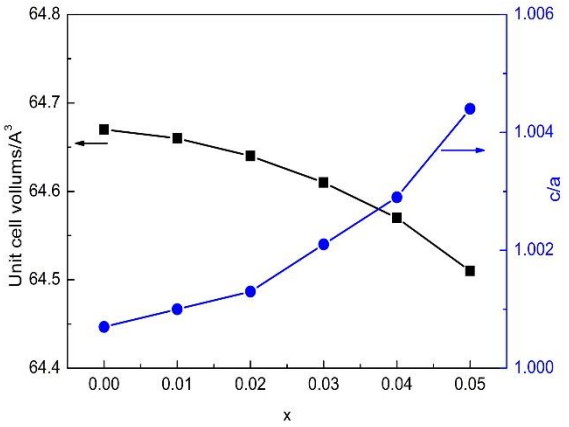

Figure 2. Variations of the unit cell volume and the c/a ratio of the ceramics with different x calculated according to the XRD data.

Fig. 2 shows the variations of the unit cell volume and the c/a ratio of the ceramics with different x calculated according to the XRD data. Stronger tetragonality with the increasing x was observed, which can be attributed to the elongated *c* axis lattice constant and the shortened *a* axis lattice constant.

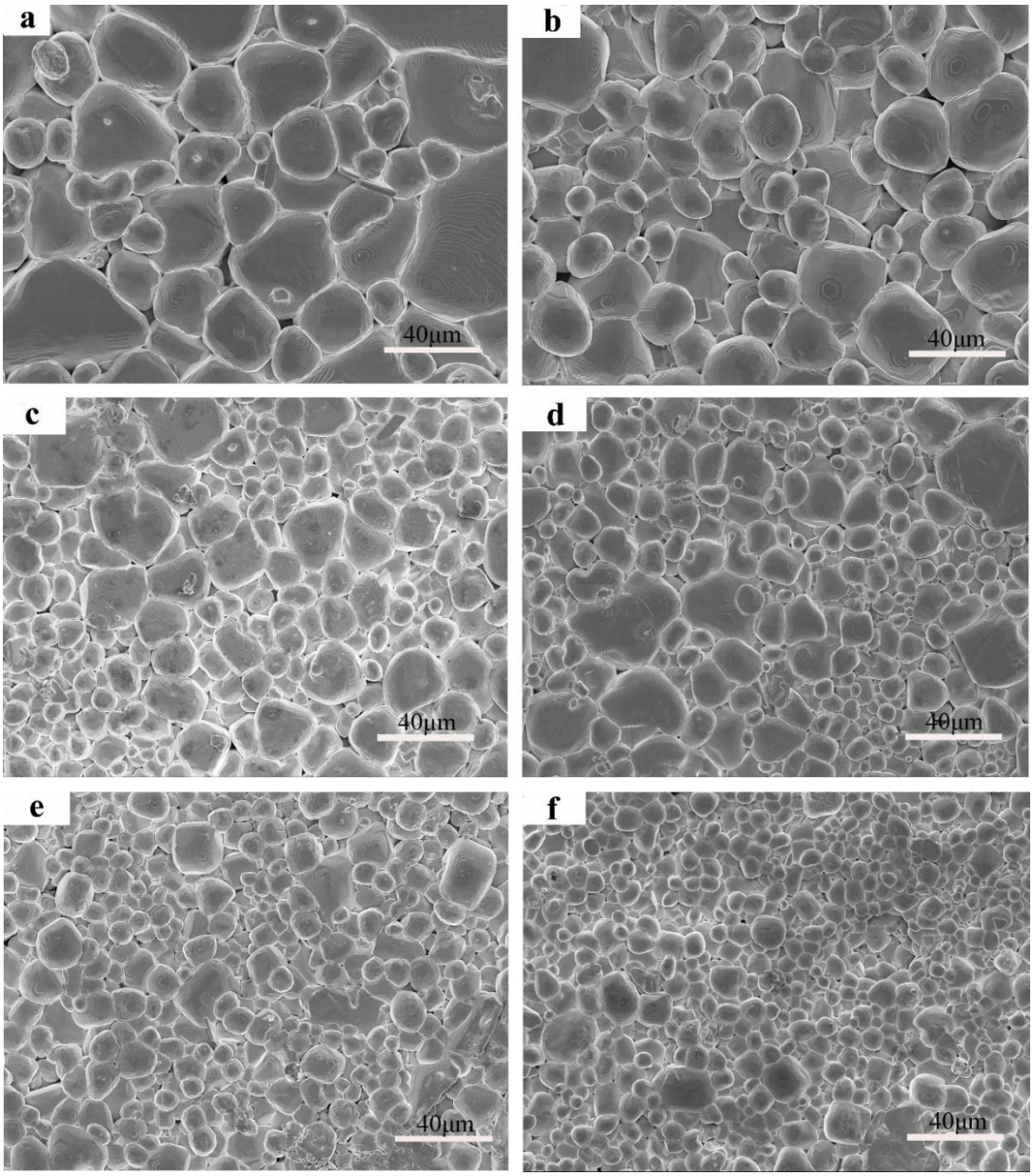

Figure 3. SEM images of the BCTS-Ce-xNd_2O_3 ceramics. a. x= 0; b. x=0.01; c. x=0.02 d. x=0.03; e. x=0.04; f. x=0.05.

It is also notable that the XRD patterns shift slightly to the right derived from the shrinkage of the unit cell volume. It has been approved in literatures by Raman tests and XPS results that Ce^{3+} ions mainly substitute for Ba^{2+} sites [21, 24]. The deformation in the BCTS lattice should not be attributed to the substitution of Ce^{3+} ions due to the radius similarity of Ce^{3+} (1.34 Å) [20] and Ba^{2+} (1.35Å) [25]. Therefore, the decreased unit cell volumes observed in Fig. 2 can be attributed to the doping of Nd^{3+} (0.995 Å) ions in Ba^{2+} sites of the perovskite structure [26]. The tetragonality (c/a) gradually increases

with x, indicating that the variation of cell volume does not make major structural changes in the tetragonal shape of the BCTS composition. The variations of the lattice parameters can be attributed to the symmetry changing in the BCTS-Ce- xNd_2O_3 structures.

Fig. 3 presents SEM images of the BCTS-Ce-xNd_2O_3 ceramics. More uniformly distributed microstructures were observed with the addition of Nd_2O_3. The average grain sizes and the relative densities of the ceramics with different x were summarized in Fig. 4. The densities of the samples were also listed in Table 1. The relative density varies from 92.3% (x=0), 91.6% (x=0.01), 92.5% (x=0.02), 91.3% (x=0.03) and 90.6% (x=0.04) to 90.1%(x=0.05), respectively. The decrease of the densities in the samples with x>0.02 suggests that the addition of appropriate amount of Nd_2O_3 is beneficial to motivate the formation of homogeneous microstructures during sintering. The corresponding average grain sizes obviously decrease from 68.7μm at x=0 to 17.1μm at x=0.05. It can be attributed to the pinning effect with the addition of Nd_2O_3 [22, 23, 27].

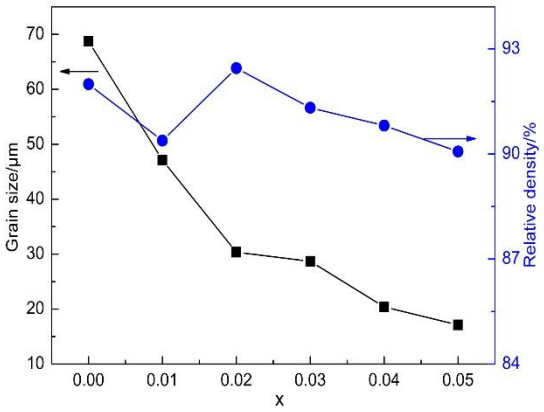

Figure 4. The average grain sizes and the relative densities of the BCTS-Ce-xNd_2O_3 ceramics changing with x.

Table 1. Densities of the BCTS-Ce-xNd_2O_3 ceramics with different x.

Nd content / mol%	0	0.01	0.02	0.03	0.04	0.05
Density / g·cm^{-3}	5.7972	5.8823	5.9129	5.9747	5.9871	6.0248
TD / g·cm^{-3}	5.3332	5.3167	5.4664	5.4561	5.4361	5.4203
RD / %	91.99	90.38	92.45	91.32	90.81	90.07

Fig. 5 shows the piezoelectric coefficient (d_{33}) and planar mode electromechanical coupling coefficient (K_p) of the BCTS-Ce-xNd_2O_3 ceramics. The d_{33} value for pure BCTS system was achieved as 436 pC/N in our previous work [22]. The addition of 0.03mol% CeO_2 increased the value to 481 pC/N, corresponding to the sample of x=0. The d_{33} value keeps increasing with the addition of Nd_2O_3 and reaches the maximum value of 578 pC/N at x=0.03 then decreases to 445 pC/N at x=0.05. Similar changing tendency is observed in K_p, which reaches to the maximum value of 49.6% at x=0.03. The remarkable improvement of d_{33} is related to the morphotropic phase boundary (MPB) effect, around

where domain is easily to rotate due to the low energy barrier during polarization process [9, 28, 29]. The A-site substitution by Nd^{3+} ions in the BCTS structures also contributes to the piezoelectric properties improvement. The Nd^{3+}-barium vacancies can be generated during the A-site substitution according to the defect chemistry in Nd^{3+} doped $BaTiO_3$ system [24, 25], which decrease strain energy and promote the movement of the domains [30]. The piezoelectric properties begin to be deteriorated obviously at x>0.03, which is related to the apparent grain size decreasing after this point. Liu and Randall [31, 32] reported that the domain size decreases with the reducing of grain size in perovskite-type ferroelectrics. The domain walls with small scales become more difficult to change direction in polarization process, leading to the decrease of the piezoelectric properties [33,34].

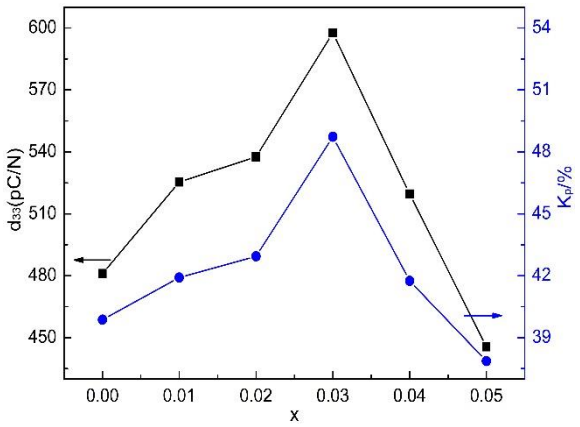

Figure 5. The piezoelectric coefficient (d_{33}) and planar mode electromechanical coupling coefficient (K_p) of the BCTS-Ce-xNd_2O_3 ceramics with x=0-0.05.

Fig. 6 shows the temperature dependence of the dielectric constant (ε_r) and dielectric loss factor of the samples at 1kHz. The dielectric peak broadening with x increasing from 0.02 to 0.05 confirmed the polymorphic phase transitions from the rhombohedral phase to the ferroelectric tetragonal phase (T_{R-T}). The peak broadening may cause the polarization fluctuation or spatial composition fluctuation in bulk samples [27]. The dielectric constant increases with x and reaches the maximum value at x=0.03 then decreases. It can be attributed to the large local random electrical field and strain field in the crystal lattice. Simultaneously, the higher dielectric constant is beneficial to the application of the ceramic capacitors. The characteristic of the dielectric loss is similar to that of the dielectric constant due to the homogeneous microstructures of the ceramics.

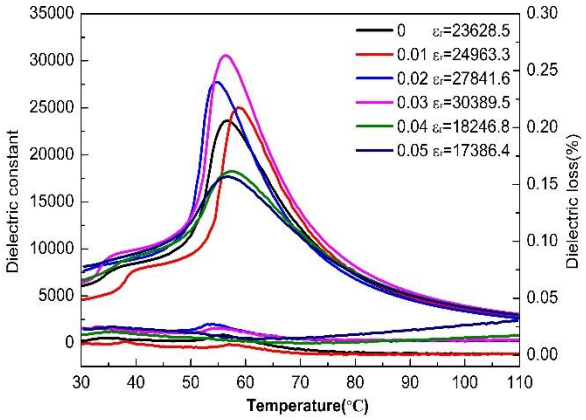

Figure 6. Temperature dependence of the dielectric constant and dielectric loss factor of the BCTS-Ce-xNd_2O_3 ceramics with x=0-0.05 at 1 kHz.

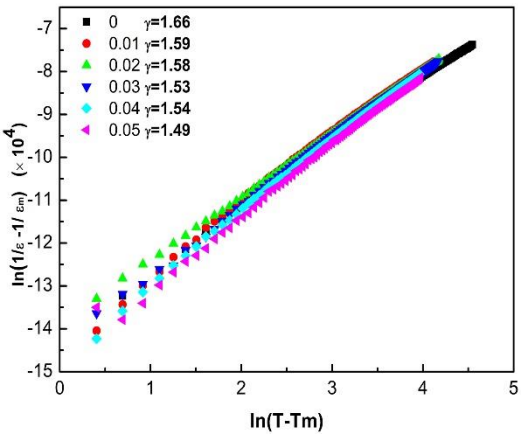

Figure 7. Plots of $\ln(1/\varepsilon-1/\varepsilon_m)$ versus $\ln(T-T_m)$ of the BCTS-Ce-xNd_2O_3 ceramics with different x according to dielectric constant fitting.

A modified empirical expression [35, 36] was introduced to further characterize the dielectric properites:

$$1/\varepsilon-1/\varepsilon_m=(T-T_m)^{\gamma}C^{-1} \qquad (2)$$

Wherein, C is a Curie-like constant and γ is the diffuseness exponent of the phase transition and representing the degree of relaxation. The γ value is obtained from the fitting of experimental data, which normally changes from 1 to 2, corresponding to the normal ferroelectric and the completely disordered relaxor ferroelectric.

Fig. 7 shows plots of $\ln(1/\varepsilon-1/\varepsilon_m)$ versus ln(T -Tm) of samples with different x according to dielectric constant fitting. The corresponding γ value decreased gradually from 1.66, 1.59, 1.58, 1.53, 1.54 to 1.49. The changing tendency is indicative of weakened diffuse phase transition behavior with x increasing. The substitution in A-sites by both Ce and Nd ions might hinder long-range ordering, thus produce polar nano-regions and result in diffuseness [35]. Additionally, fine grain sizes change the balance between the long-range and short-range forces, which resulting in larger relaxor state and diffuseness [36, 37].

Fig. 8 shows the polarization-electric field hysteresis loops of the BCTS-Ce-xNd_2O_3 ceramics at room temperature. **Fig. 9** presents the remnant polarization (P_r) and the coercive field (E_c) of the samples as a function of x. P_r decreased and E_c increased gradually with x increasing. Slight asymmetry in the polarization-electric field hysteresis loops may be derived to the existence of crystal defects and space-charge field [14]. As discussed in Y_2O_3 doped $Ba_{0.9}Ca_{0.1}Ti_{0.9}Sn_{0.1}O_3$ ceramics in our previous work [17], the number of grains participating in polarization reverse has the same changing tendency with grain size at fixed temperature. According to Avrami model for ferroelectrics [38], the changing of grain size influence the proportion of grains contributing in polarization reverse at fixed temperature [39]. The decrease of the grains number led to the declination in P_r, and the increased energy barriers resulted in the increase in E_c. The saturated and "soft" polarization-electric field hysteresis loops make it feasible to obtain excellent piezoelectric properties by tailoring the poling condition.

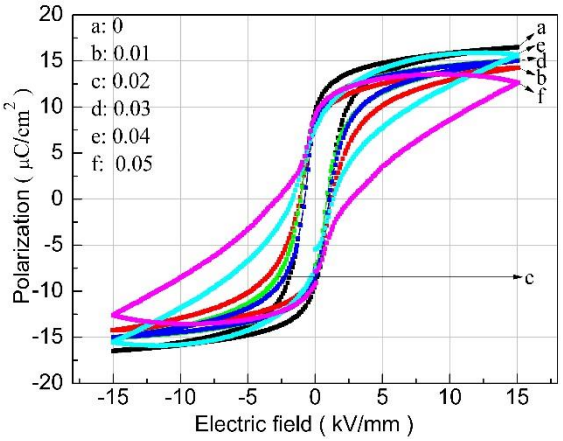

Figure 8. Polarization-electric field hysteresis loops of the BCTS-Ce-xNd_2O_3 ceramics with different x measured at room temperature (10 Hz, 3.5 kV/mm).

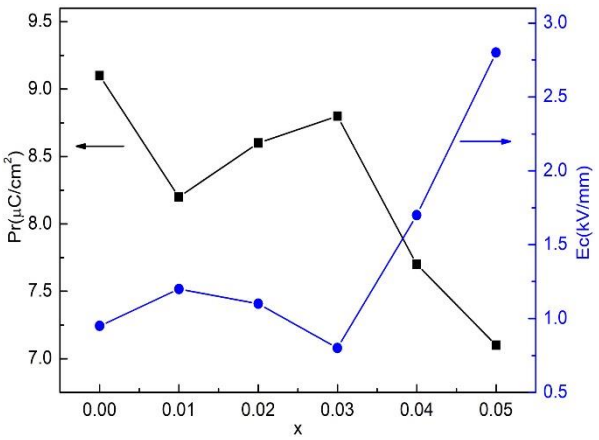

Figure 9. The remnant polarization (P_r)and the coercive field (E_c) of the ceramics with different x.

4. CONCLUSIONS

$Ba_{0.94}Ca_{0.06}Ti_{0.9}Sn_{0.10}O_3$-0.03mol%$CeO_2$-xmol%$Nd_2O_3$ (x=0-0.05) piezoelectric ceramics were fabricated by solid-state sintering method. All the ceramics samples showed single perovskite structure with no secondary phase. Tetragonal and rhombohedral phases coexisted in the composition from x=0.02 to 0.05. The grain size of the samples decreased from 68.7μm to 17.1μm. The piezoelectric properties were optimized at x=0.03 with d_{33} of 578 pC/N and K_P of 49.0%. The typical diffuse phase transition behavior was weakened with the addition of Nd_2O_3. These results indicate that the improvement on the electric properties of the BCTS ceramics, especially on piezoelectric properties may provide a possibility to break through the bottleneck of the application of $BaTiO_3$ based lead-free ceramics.

ACKNOWLEDGEMENT
The authors wish to acknowledge the financial support of National Natural Science Foundation of China (Grant No. 51702024).

References

1. P. Sharma, N. Berwal, N. Ahlawat, A.S. Maan and R. Punia, *Ceramics International*, 15 (2019) 20368.
2. K. Xu, J. Li, X. Lv, J. G. Wu, X. X. Zhang, D. Q. Xiao and J. G. Zhu, *Advanced. Material*., 28 (2016) 8519.
3. X. Lv, J. G Wu, C. L. Zhao, D. Q. Xiao, J. G. Zhu, Z. H. Zhang, C. H. Zhang and X. X. Zhang, *Journal of European Ceramic. Society.,* 39 (2019) 305.
4. C. L. Zhao, B. Wu, H. C. Thong and J. G. Wu, *Journal of European Ceramic Society*, 38 (2018) 5411.
5. A. Rambabu and K. C. RajuTrans, *Transactions of the Indian Ceramic Society*, 70(3) (2011) 135.
6. J. G. Wu, D. Q. Xiao and J. G. Zhu., *Journal of Material Science: Material Electronic,* 26 (2015) 9297.
7. G. Chen, C. Y. Deng, X. D. Peng, C. L. Fu, W. Cai, R. L. Gao and X. L. Deng, *Transactions of the Indian Ceramic Society*, 75(4) (2016) 220.
8. X. Chen, X. Z. Ruan, K. Y. Zhao, X. Q. He, J. T. Zeng, Y. S. Li, L. Y. Zheng, C. H. Park and G. R .Li, *Journal of Alloys and Compounds,* 632(2015) 103.
9. Y. Yang, H. Hao, L. Zhang, C. Chen, Z. Q. Luo, Z. Liu, Z. H. Yao, M. H. Cao and H. X. Liu, *Ceramics International*, 44 (2018) 11109.
10. P. Wang, Y. X. Li and Y. Q. Lu, *Journal of European Ceramic. Society.*, 31 (2011) 2005.
11. Y. L. Huang, C. L. Zhao, X. Lv, H. Wang and J. G. Wu, *Ceramics International*, 43 (2017) 13516.
12. L. Zhao, B. P. Zhang, P. F. Zhou, L. F. Zhu and N. Wang, *Ceramics International,* 42 (2016) 1086.
13. L. F. Zhu, B. P. Zhang, X. K. Zhao, L. Zhao, P. F. Zhou and J. F. Li, *Journal of the American Ceramic Society,* 96 (2013) 241.
14. Z. H. Chen, Z. W. Li, C. Fang, J. H. Qiu, J. N. Ding, W. Q. Zhu and J. J. Xu, *Journal of Physics Chemistry Solids,* 111 (2017) 311.
15. C. Han, J. G. Wu, C. H. Pu, S. Qiao, B. Wu, J. G. Zhu and D. Q. Xiao, *Ceramics International,* 38 (2012) 6359.
16. J. Wu, W. J. Mao, Z. Wu and Y. M. Jia, *Material Letters*, 166 (2016) 75.
17. Z. H. Chen, Z. W. Li, J. H. Qiu, T. X. Zhao, K. Q. Zhu, J. N. Ding, W. Q. Zhu and J. J. Xu, *Physics Status Solidi A,* 170 (2017) 0417.
18. Z. H. Chen, Z. W. Li, J. H. Qiu, T. X. Zhao, J. N. Ding, X. G. Jia and J. J. Xu, *Journal of European*

Ceramic Society, 38 (2018) 1349.
19. Z. H. Chen, Z. W. Li, J. N. Ding, J. J. Xu and J. H. Qiu, Y. Yang, *Journal of Alloys and Compound*s, 704 (2017) 141.
20. S. Yasmin, S. Choudhury, M.A. Hakim, A.H. Bhuiyan and M.J. Rahman, *Journal of Materials Science and Technology*, 27(8) (2011) 759.
21. J. H. Shi and W. M. Yang, *Journal of Alloys and Compound*s, 472 (2009) 267.
22. Y. R. Cui, X. Y. Liu, M. H. Jiang, X. Y. Zhao, X. Shan, W. H. Li and C. L. Yuan, *Ceramics International*, 384 (2012) 761.
23. Z. H. Chen, Z. W. Li, J. J. Xu, H. F. Guo, B. Zhang, J. N. Ding and J. H. Qiu, *Journal of Alloys and Compound*s, 720 (2017) 562.
24. P. Q. Long, X. T. Liu, X. Long and Z. G. Yi, *Journal of Alloys and Compound*s, 706 (2017) 234.
25. Z. Yao, H. Liu, Y. Liu, Z. Wu and Z. Shen, *Chemical Physics*, 109 (2008) 475.
26. S. J. Liu, L. X. Zhang, J. Q. Wang, Y. Y. Zhao and X. Wang, *Ceramics International*, 43 (2017) 10683.
27. Z. H. Chen, Z. W. Li, M. G. Ma, T. X. Zhao, J. H. Qiu and J. N. Ding, *Journal of Rare Earths*, 36 (2018) 745.
28. S. J. Liu, L. X. Zhang, J. P. Wang, Y. Y. Zhang and X. Wang, *Ceramics International*, 43 (2017) 10683.
29. Y. R. Cui, X. Y. Liu, M. H. Jiang, X. Y. Zhao, X. Shan, W. H. Li, C. L. Yuan, C. R. Zhou, *Ceramics International*, 38 (2012) 4761.
30. D. Pamu, G. Lakshmi Narayana Rao and K. C. James Raju, *Transactions of the Indian Ceramic Society*, 67 (4) (2008) 211.
31. M. Zannen, A. Lahmar, M. Dietze., H. Khenmakhem, *Materials Chemical and Physics*,134 (2012) 829.
32. C. A. Randall, N. C. Kim, J. P. Kucera, W. W. Cao and T. R. Shrout, *Journal of the American Ceramic Society*, 81 (1998) 677.
33. X. Liu, Z. H. Chen, B. J. Fang, J. N. Ding, X. Y. Zhao, H. Q. Xu and H. S. Luo, *Journal of Alloys and Compound*s, 640 (2015) 128.
34. J. H. Jeong, M. G. Park and Y. H .Han, *Journal of Electroceramics*, 13 (2004) 805.
35. D. W. Wang, A. Khesro, S. Murakami, A. Feteira, Q. L. Zhao and I. Reaney, *Journal of European Ceramic Society*, 37 (2017) 1857-1860.
36. J. G. Hao, W. F. Bai, W. Li and J. W. Zhai, *Journal of the American Ceramic Society*, 95 (2012) 1998.
37. K. J. Uchino and S. Nomura, *Ferroelectrics Letters Section*, 44 (1982) 55.
38. N. Horchidan, A. Ianculescu, C. Vasilescu, M. Deluca and V. Musteata, *Journal of European Ceramic Society*, 34 (2014) 3661.
39. H. Orihara, S. Hashimoto, Y. Ishibashi, *Journal of the Physical Society Japan*, 63 (1994) 1031.